ISBN: 978-3-95450-247-9 ISSN: 2673-5490 doi: 10.18429/JACoW-IPAC2024-TUPC44

SINGLE BUNCH TRACKING ON THE TEN-PASS ER@CEBAF ENERGY RECOVERY BEAMLINE*

I. Neththikumara† [1,2], T. Satogata[1,2], S.A. Bogacz[1], R. Gamage[1]
[1] Thomas Jefferson National Accelerator Facility, Newport News, USA
[2] Center for Accelerator Studies, Old Dominion University, Norfolk, USA

Abstract

The proposed ten-pass energy recovery linac (ERL) demonstration (five accelerating, five decelerating) at the CEBAF accelerator, ER@CEBAF, involves a multi-GeV energy range of a continuous electron beam. New CEBAF transverse optics were designed for this ERL demonstration. This redesign incorporates additional components in Arc A, including a path length chicane and new quadrupoles to ensure proper dispersion localization. The new five energy recovery passes with a shared arc transport scheme challenge the overall beamline optics design, including large beta functions in the CEBAF spreaders and recombiners. Here we discuss results of bunch tracking performed using the elegant tracking code for the full ER@CEBAF beamline.

INTRODUCTION

The Continuous Electron Beam Accelerator Facility (CEBAF) at Jefferson lab utilizes superconducting radio frequency (SRF) technology for accelerating polarized electron beam. CEBAF features a racetrack-shaped geometry, consisting of two SRF linacs (North and South linacs) connected with two sets of vertically stacked arc segments namely East and West arcs. Each linac is capable of accelerating electron beam up to 1.09 GeV per pass. The accelerated electron beams are directed towards four experimental halls, designated as Hall A, B, C, and D located at the end of the linacs, as illustrated in Fig. 1 [1].

Implementing recirculating energy recovery passes necessitates the installation of two primary hardware segments. First, a pathlength chicane to introduce an additional path length difference of 10 cm, equal to half of the CEBAF RF wavelength. This will be installed within the highest energy arc, Arc A. Secondly, a low energy beam dump is required to dispose of the low energy beam after energy recovery. This will be located at the end of the last linac pass, i.e. at the end of the South linac. Preliminary studies indicated that the maximum feasible energy gain per linac pass to accommodate 5-ER passes is 750 MeV, implying a feasible upper energy limit of 7.5 GeV. These values are obtained to achieve an optimum balance between maximizing energy reach and mitigating beam energy spread due to emission of synchrotron radiation in higher energy arcs, constrained by energy acceptance.

* This material is based upon work supported by the U.S. Department of Energy under contract DE-AC05-06OR23177.
† isurunh@jlab.org

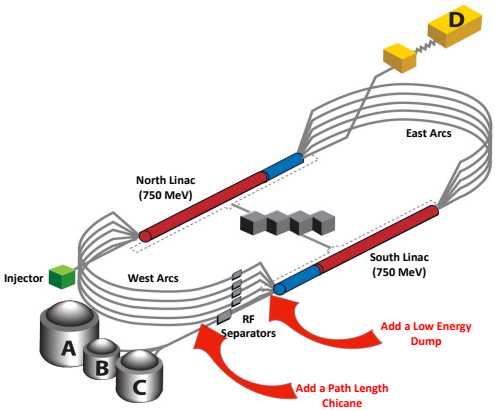

Figure 1: Layout of the CEBAF accelerator, indicating additions for ER@CEBAF.

TEN PASS BEAMLINE

The beamline comprised of 5-accelerating and 5-energy recovery passes was designed using elegant [2]. Linac optics were obtained using a special 10-pass linac lattice arrangement and utilizing multi-objective genetic optimization methods [3]. The pathlength chicane has total length of 32 m, added in the extraction region of Arc A. This 4-dipole chicane consists of two dogleg, extending approximately 1.2 m into the tunnel aisle. This can be installed while maintaining sufficient space for equipment installation and egress safety [4]. Furthermore, the spreader and recombiner regions of this Arc A were updated in the model with multiple quadrupole magnets to achieve localized dispersions. With these modifications, the optics of the 10 ER@CEBAF arcs were redesigned to increase the momentum acceptance for the decelerating beamline in this shared beam transportation scheme [4]. The Twiss diagrams for the redesigned beamline are provided in [5]. The complete beamline is approximately 12 500 m long, with the highest $\beta(s)$ peak of approximately 1200 m observed at Arc 7.

SINGLE BUNCH TRACKING RESULTS

Preliminary particle tracking analysis has been conducted on this redesigned beamline using a single bunch with a Gaussian profile. The initial beam parameters used are listed in Table 1.

Beam Energy Comparison

At higher energies, synchrotron radiation effects constitutes a critical factor in this recirculating energy recovery

ISBN: 978-3-95450-247-9 ISSN: 2673-5490 doi: 10.18429/JACoW-IPAC2024-TUPC44

Table 1: Initial Beam Parameters for ER@CEBAF Tracking

Parameter	Value
Bunch current	100 µA
Bunch length	0.1 mm
Energy spread	2×10^{-5}
$\epsilon_{(x,y)}$	4×10^{-9} m

Table 2: Energy Loss and Cumulative Energy Loss After Each Arc in the 10-Pass Beamline

Arc	ΔE_{Acc} [MeV]	ΔE_{Dec} [MeV]	$\Delta E_{cum(Acc,Dec)}$ [MeV]
Arc 1	0.010	0.009	0.010, 24.665
Arc 2	0.047	0.044	0.057, 24.665
Arc 3	0.181	0.173	0.238, 24.611
Arc 4	0.295	0.286	0.533, 24.438
Arc 5	0.647	0.632	1.180, 24.152
Arc 6	1.222	1.200	2.402, 23.520
Arc 7	1.475	1.455	3.561, 22.320
Arc 8	2.421	2.398	6.298, 20.866
Arc 9	3.561	3.546	9.856, 18.467
Arc A	5.063	N/A	14.922, N/A

beamline. Substantial beam energy losses are observed within the arcs where the electron beam energy is highest. Table 2 lists these energy losses observed from a bunch consisting of 1024 particles.

The energy of the beam upon exiting from the south linac after energy recovery is 60.12 MeV with a total energy loss of 25 MeV from synchrotron radiation emission as listed in Table 2. A comparison plot of the design and beam energy is shown in Fig. 2. Here, the vertical dashed line indicates the end of the accelerating beamline, which is the beginning of arc A. There is not significant energy difference visible on this plot due to the large energy scale of the design.

Beam Optics Comparison

Optics comparisons were performed with a bunch consisting of 10^5 particles to reduce statistical errors in beam parameter calculations.

The design and beam $\beta(s)$ variation is compared in Fig. 3. The same vertical scale is utilized for both plots representing x & y $\beta(s)$ variations, to facilitate with a clear visual comparison. The vertical beam $\beta(s)$ closely follows the design, whereas in horizontal plane, slightly larger beam $\beta(s)$ variations are observed within arcs, notably within spreader and recombiner regions. The sharp peaks in these regions imply strong focusing necessitating meticulous beam transport control [5].

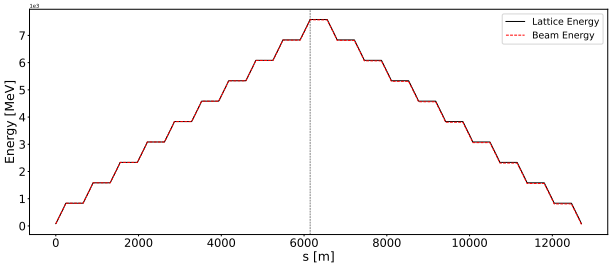

Figure 2: The energy profiles of the beam and lattice, through the 10-pass beamline.

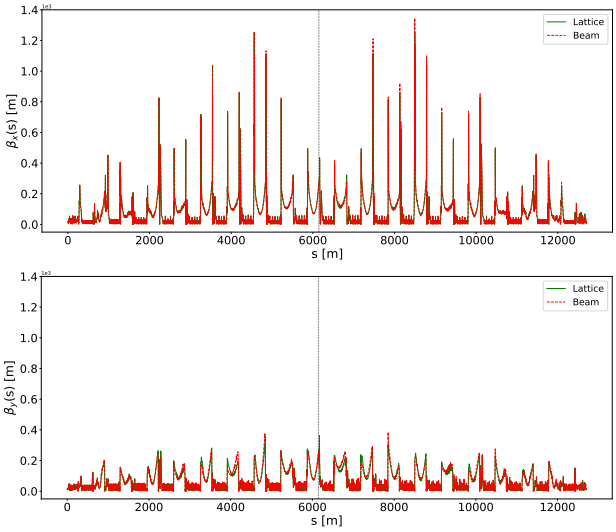

Figure 3: The horizontal and vertical $\beta(s)$ variation through the 10-pass beamline.

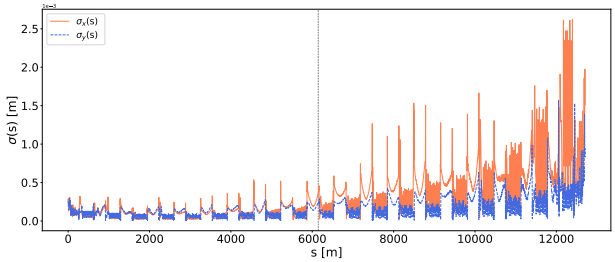

Figure 4: Horizontal and vertical beam size $\sigma(s)$ variation through the 10-pass beamline.

Beam Size Evolution

The horizontal and vertical beam size variations through the beamline are illustrated in Fig. 4. Beam sizes consistently remain smaller throughout the accelerating beamline, but the horizontal beam size slightly increases as the beam travels through horizontally bending beamline. Within the decelerating beamline, both the horizontal and vertical beam sizes experiences a more substantial increase due to accumulated emittance growth. The maximum observed beam size in either plane is approximately 2.5 mm which is comparably smaller than the aperture of beam pipes.

Beam sizes $\sigma_{x,y}$ depends on the emittances $\epsilon_{x,y}$, Twiss parameters $\beta_{x,y}(s)$, dispersions $D_{x,y}(s)$ and fractional momentum offset δ through [6]:

$$\sigma_{x,y}(s) = \sqrt{\epsilon_{x,y}\beta_{x,y} + D_{x,y}^2\delta^2}\,. \quad (1)$$

The fractional momentum spread σ_δ of the beam increases in the arcs due to synchrotron radiation. Adiabatic damping from acceleration reduces it during accel-

ISBN: 978-3-95450-247-9 ISSN: 2673-5490 doi: 10.18429/JACoW-IPAC2024-TUPC44

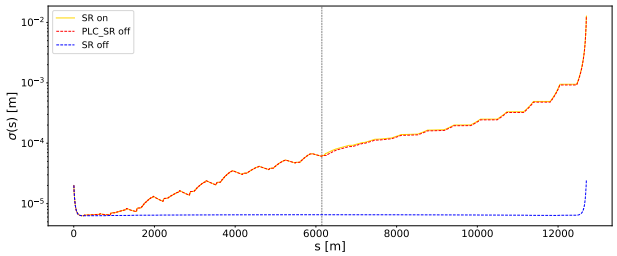

Figure 5: The beam fractional momentum spread (σ_δ) variation through the 10-pass beamline.

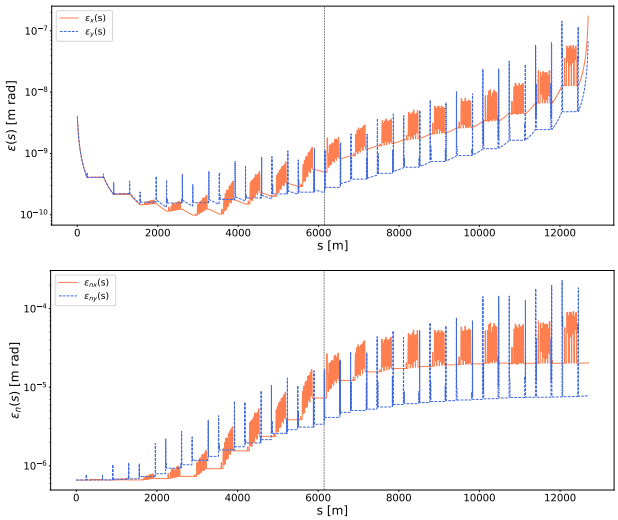

Figure 6: The horizontal and vertical beam emittances (top: geometric $\epsilon_{x,y}$; bottom: normalized $\epsilon_{x,y;n}$) through the 10-pass beamline.

eration, but it returns and increases during deceleration, producing the fractional momentum offset variation shown in Fig. 5. The blue curve represent $\sigma_\delta(s)$ variation with no synchrotron radiation effects, shows a symmetric fractional energy spread variation as expected in an ideal ERL. The yellow and red curves illustrate energy spread variation with synchrotron radiation effects, with and without the inclusion of SR effects for the path length chicane dipoles respectively. This observation suggests the need of proper energy compensation mechanism.

Beam Emittance Evolution

This beamline combines linacs passes phased to accelerate the beam, 180 degree arcs and vertical splitters/recombiners to transport different beam energies, and linac passes phased to decelerate the beam. Geometric emittance ϵ scales inversely with the beam energy p, leading to a rough scaling of beam size $\sigma_{x,y}$ with inverse $\sqrt{p}$:

$$\epsilon \propto \frac{1}{p} \quad \Rightarrow \quad \sigma_{x,y} \propto \frac{1}{\sqrt{p}} \,. \tag{2}$$

The beam emittance evolution therefore varies in a somewhat unusual way: adiabatic damping dominates low-energy linac acceleration passes, synchrotron radiation driving emittance growth dominates higher energies for acceleration and deceleration, and adiabatic *un*damping dominates the final linac deceleration passes.

Figure 6 illustrates the variation of emittances throughout this beamline. The top plot shows the geometric emittance $\epsilon_{x,y}$, while the bottom plot the normalized emittance $\epsilon_{x,y;n}$. A reduction of geometric emittance can be seen during accelerating linac passes from adiabatic damping, and an increase during decelerating passes from adiabatic undamping. Normalized emittances remains constant through the accelerating and decelerating linacs, but exhibit an increase within arcs depending on beam energy and synchrotron radiation.

CONCLUSION

A close alignment between the design and the beam Twiss parameters was observed through this redesigned beamline. The recorded beam sizes are comparably smaller and no particle losses were recorded. However, a significant amount of beam energy is lost due to radiation emission in arcs, causing larger beam energy spread in the ER passes. Moreover this results a larger beam sizes within the ER passes. Hence a proper energy compensation mechanism with introducing off-crest beam transportation for a chirped beam alongside employing proper bunch compression schemes is required.

Furthermore, an effective control of the energy spread is necessary to mitigate the observed growth, and this can be achieved by manipulating the longitudinal phase space.

REFERENCES

[1] S. A. Bogacz *et al.*, "ER@CEBAF:A test of 5-pass energy recovery at CEBAF" , Internal Technical Document, Collider-Accelerator Department, Brookhaven National Laboratory, 2016.

[2] M. Borland, "elegant: A flexible SDDS-compliant code for accelerator simulation", Advanced Photon Source LS-287, September 2000. doi:10.2172/761286

[3] I. Neththikumara, T. Satogata, S. A. Bogacz, R. M. Bodenstein, and A. Vandenhoeke, "Linac optics optimization with multi-objective optimization", in *Proc. IPAC'22*, Bangkok, Thailand, May 2022. doi:10.18429/JACoW-IPAC2022-MOPOTK050

[4] I. Neththikumara, S. A. Bogacz, and T. Satogata, "Re-design of CEBAF optics for ER@CEBAF", in *Proc. IPAC'23*, Venice, Italy, May 2023. doi:10.18429/JACoW-IPAC2023-WEPL056

[5] I. Neththikumara, "Optics studies for multipass energy recovery at CEBAF: ER@CEBAF",(PhD), PhD Dissertation, Physics, Old Dominion University, December 2023. doi:10.25777/prn7-e491

[6] H. Wiedemann, "Particle Accelerator Physics", Springer Cham, 2007. doi:10.1007/978-3-319-18317-6